Rust-Based Catalysts Under Thermal Influence In Heterogeneous Photo-Fenton Process For Improving Removal Of Linear Alkylbenzene Sulfonate From Laundry Effluent At Near Neutral PH

Endang Tri Wahyuni[1*], Jeannina Cahyo Rani[1], Fifi Aulia Yahya[1], Early Zahwa Alharissa[2], Suherman Suherman[1], and Nur Farhana Jaafar[3]

[1] *Department of Chemistry, Faculty of Mathematic and Natural Sciences, Universitas Gadjah Mada, Sekip Utara POB Bls 21 Yogyakarta, Indonesia*
[2] *Research Center for Nanoscience and Nanotechnology, Institut Teknologi Bandung, Indonesia*
[3] *School of Chemical Sciences, 11800 Universiti Sains Malaysia (USM) Pulau Pinang, Malaysia*
[*] *Corresponding author. E-mail: endang$_t$riw@ugm.ac.id*

Received: Jan. 07, 2026; Accepted: Mar. 23, 2026

Water pollution caused by linear alkylbenzene sulfonate (LAS) from laundry effluent has been increasingly detected, posing serious threats to both the environment and human health. Preventing this pollution requires a method that not only effectively reduces LAS concentration but also transforms it into smaller, safer molecules. This research aims to enhance the effectiveness of the photo-Fenton process at near-neutral pH for the removal of LAS from laundry effluent by introducing rusted iron waste as a heterogeneous catalyst thermally treated at 100 °C and 450 °C. LAS photodegradation was conducted using a batch technique along with optimization of several process variables. The systematic characterization using XRD, DR-UV/Visible, SEM, and surface area analyzer techniques confirmed that increasing the calcination temperature of rusty waste results in the formation of more crystalline and purer iron oxide (Fe_2O_3) exhibiting larger surface areas, wider pore diameters, and smaller band gap energies. Consistent with these properties, the iron oxide catalyst was able to remove LAS from laundry wastewater at an initial concentration of 119.18mg/L, achieving up to 95% degradation efficiency, significantly higher than catalysts prepared at lower temperatures. The optimal degradation condition for 50 mL of wastewater was obtained by applying 6 g L^{-1} catalyst dose and 250 mmolL^{-1} of H_2O_2 at pH 6 , resulting in a 95% reduction of LAS within 60 minutes. These findings demonstrate that the heterogeneous photo-Fenton process, employing low-cost rust-derived iron oxide catalysts under near-neutral pH conditions, provides an effective and environmentally sustainable approach for treating laundry wastewater. Consequently, this method holds great potential in mitigating environmental pollution.

Keywords: laundry effluent; photo-Fenton; iron rust; solid catalyst; neutral pH

http://dx.doi.org/10.6180/jase.202609_32.038

1. Introduction

Laundry services are widely found in both urban and rural communities, generating and discharging large volumes of wastewater with high concentrations of linear alkylbenzene sulfonates (LAS) [1–4]. As is known, laundry activities not only require large amounts of rinsing water but also consistently use detergent in substantial quantities [1–4]. The main active component in the detergent is anionic surfactants such as LAS [1–5]. Wastewater with high LAS content is also found in the detergent manufacturing industry [5–10]. The discharge of such wastewater without prior

treatment may cause environmental pollution by LAS.

In the environment, LAS is a persistent organic pollutant that is difficult to degrade and thus tends to accumulate at high concentrations [1–10]. In aquatic ecosystems, LAS exhibits toxic effects on living organisms, disrupting biological cycles and ultimately leading to environmental damage[1–10]. Humans accidentally consuming food or beverages contaminated with LAS, even at low concentrations, may experience nausea, vomiting, and other health problems [9, 10]. Therefore, reducing LAS concentrations in laundry wastewater is of critical importance.

The removal of LAS from laundry wastewater has been reported to be effectively achieved by degradation into smaller molecules using the photo-Fenton method [7, 8]. Photo-Fenton process is a type of advanced oxidation process (AOP) in which hydroxyl radicals (·OH) are produced through the reaction of the dissolved Fe(II) ions with hydrogen peroxide (H_2O_2) under UV irradiation, which is also known as homogeneous photo-Fenton. The reaction taken palce in the homogenous photo-Fenton are presented as reactions (1-3) [7, 8, 11–32]:

$$Fe^{2+} + H_2O_2 \rightarrow Fe^{3+} + {}^{\cdot}OH + {}^{-}OH \quad (1)$$

$$Fe^{3+} + H_2O_2 \rightarrow Fe^{2+} + {}^{\cdot}O_2H + H^{+} \quad (2)$$

$$H_2O_2 + \text{ light } \rightarrow 2\,{}^{\cdot}OH \quad (3)$$

Hydroxyl radicals (·OH) exhibit an exceptionally high oxidation potential (E°) as high 2.8 V [12–14, 18], underscoring their strong oxidizing activity. Commonly referred to as the homogeneous photo-Fenton process, this technique is well known for its remarkable oxidative efficiency [11–32].

In addition to oxidizing As(III) to As(V) [15] and Pb(II) into Pb(IV) [16], hydroxyl radicals in the photo-Fenton process can degrade various stable organic compounds [11–13], enabling them to be widely applied in the degradation of toxic organic pollutants including anionic surfactant such as LAS [7, 8], dyes [12], antibiotics [13], p-nitrophenol [14], and pharmaceuticals residual [17].

The homogeneous photo-Fenton process exhibits optimal performance at approximately pH 3 [3, 7, 8, 11–32]. At higher pH values, its efficiency decreases markedly due to the formation of $Fe(OH)_3$ precipitates. These precipitates limit the interaction between the Fenton reagents (Fe^{2+} and H_2O_2) and light, thereby reducing the generation of hydroxyl radicals [3, 7, 8, 11–32].

Since laundry wastewater generally has a pH ranging from 5 to 7, or near neutral pH [2, 3], the homogeneous photo-Fenton method is found to be less effective for treating wastewaters [3, 8, 15, 16] [3, 8, 15-16]. Moreover, the large amounts of $Fe(OH)_3$, precipitate produced in the homogeneous photo-Fenton process, generate sludge as secondary waste, creating additional environmental problems [13, 17–32].

Considering its high efficiency in organic pollutant removal and its relatively simple process, enhancing the performance of photo-Fenton at near-neutral pH is essential. One approach is to replace soluble Fe^{2+} ions with solid iron oxide catalysts that can generate hydroxyl radicals over a wider pH range and have high chemical stability [12–32].

The solid iron-based catalysts previously studied for heterogeneous photo-Fenton processes include amorphous and crystalline iron oxides [18], magnetite (Fe_3O_4) [20], and several iron oxides synthetic [21], prepared from commercial iron have been reported. However, the catalytic efficiency of iron oxides remains unsatisfactory due to the aggregation and agglomeration of iron oxide nanoparticles leading to lower surface area [13]. An effective solution to conquer this problem is by immobilizing iron oxides on various supports such as SiO_2 [22], silica gel [23], ZSM-5 type synthetic zeolite [24], and biochar [25], have also been explored. The iron oxides and supporting solids are typically prepared from commercial salts, which are costly and consequently contribute to the high operational expenses of the heterogeneous photo-Fenton process application.

To address this weakness, natural iron-based materials, including pyrite (FeS_2) [26], chalcopyrite ($CuFeS_2$) [27], clays [28], kaolin [29], and halloysite [30], have been investigated as alternative catalyst supports. Yet, the limited availability of sulfide minerals and clays may constrain their practical applicability. A more promising alternative lies in the direct use of the support of iron-containing wastes, such as sludge from dyeing processes [31] and iron rust [32], which are both cost-effective. Among these options, iron rust is particularly advantageous due to its greater abundance and environmentally benign nature.

Iron rust is an iron oxide compound formed from the oxidation of metallic iron materials in humid air. The formation of rust leads to the iron-based materials being fragile or damaged, rendering them unusable and eventually discarded as waste [32–35]. In the environment, rust waste may diminish aesthetic value, lack economic benefit, and may even trigger tetanus infections in open wounds [33–35]. The utilization of rust, whose primary component is Fe_2O_3, has previously been reported, for instance, as a dopant source to enhance TiO_2 activity under sunlight [33–35] as well as a magnetite (Fe_3O_4) precursor for making TiO_2 recoverable [35]. Moreover, the use of iron rust as a source for synthesizing an iron oxide catalyst in heterogeneous photo-Fenton processes has been demonstrated, particularly in the decolorization of Acid Red 97 [32]. In that study, rust was firstly dissolved to obtain Fe(III) ions,

which were subsequently precipitated with hydroxide ions from a basic solution and then calcined to form iron oxide (Fe_xO_y) nanoparticles. This is not facile process and the influence of drying or calcination temperature was not investigated. In practice, these thermal conditions play a crucial role in determining the structural characteristics, optical properties, and catalytic activity of the resulting iron oxides [36–41].

Under the circumstance, this present study proposes the development of a heterogeneous photo-Fenton process employing iron rust waste as a solid catalyst to enhance the degradation efficiency of LAS in laundry discharge under near-neutral pH conditions. The rusty waste is directly utilized as a catalyst, offering a more practical approach that can be heated at either low or high temperatures. Heat treatment at different temperatures is intended to examine its influence on the physicochemical properties, which are expected to enhance the catalytic activity. This strategy also experiences in a modest way without further treatment or complexes chemicals required, unlike the previous report, which requires several methods as special treatment in utilizing iron rust source [32, 42]. Hence, this strategy leads to applying the principle of green chemistry, that are reduce the use of chemicals and additives.

Furthermore, these heterogeneous photo-Fenton experiments are conducted under varying operational parameters, including hydrogen peroxide concentration, catalyst dosage, solution pH , and irradiation time, in order to identify the optimum condition for effective LAS degradation, that can be useful as a guide for the actual application in the future.

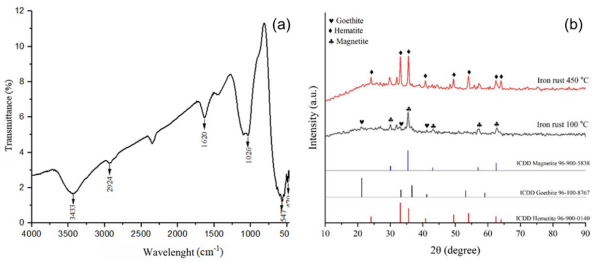

Fig. 1. (a) FTIR spectra of the original rusty waste correspond to the main functional group existed in the rusty sample, (b) XRD patterns of the dried and calcined rusty waste indicate the phase transformation of iron minerals

2. Experimental section

2.1. Research Materials

The materials used in this study include sodium dodecyl benzene sulfonate (SDBS) powder, iron(II) sulphate heptahydrate ($FeSO_4 \cdot 7H_2O$) powder, 30%w/w hydrogen peroxide (H_2O_2) solution, chloroform, and methylene blue powder. These materials were produced by Merck with pro-analysis grade quality and used without purification. The laundry wastewater was collected from one of the laundry services in Yogyakarta region, and the iron rusty waste was taken from the rusted iron of a damaged fence at UGM campus. A reactor set equipped with a Himawari UV lamp ($\lambda = 330 - 380$ nm, power $= 36$ W) was employed for conducting the photo-Fenton process.

2.2. Research procedures

2.2.1. Analysis and characterization of the iron rusty waste

The iron rusty waste that has been cleaned and milled into 200 mesh, was calcined at 450 °C for 2 hours, and the other variation was only heated at 100 °C for 2 hours. The calcined powder then was characterized using X-Ray Diffraction (4 kW with SAX and Thin Film Metrology) to identify the iron oxide typed, Fourier Transform Infrared (FTIR) spectrophotometer (Shimadzu Prestige 21) to detect the functional groups, X-Ray Fluorescence (Spectro Xepos XRF) to determine the content of the iron present, UV-Vis Diffuse Reflectance Spectroscopy (UV-Vis DRS) (UV-2401 Series) to find the band gap energy, and a Scanning Electron Microscope (Electron Probe Microanalyzer JXA-ISP 1000) to observe the morphology.

2.2.2. Analysis of laundry wastewater

The freeze-dried laundry wastewater sample was pelleted with KBr and then analyzed using FTIR. Further procedure of laundry wastewater in this experiment is enclosed in Supplementary materials.

2.2.3. Degradation of LAS using iron rusty waste in heterogeneous photo-Fenton

The wastewater (10 mL) was placed in 5 beaker glasses, and the solution pH was adjusted to be 7. Into each glass was added 110 mg of the rusty iron and 10 mL of 250 $mmolL^{-1}H_2O_2$. Next, the mixture in the beaker glasses were irradiated by a UV lamp for 60 minutes along with constant magnet stirring. When the process finished, the mixtures were filtered to get the clear solutions and then were analysed to determine the concentration of the undegraded LAS following the procedure described above. Further procedure for optimization are also conducted and explained in Supplementary section.

2.2.4. Determination of COD values

The laundry wastewater sample was measured the COD value in a bid to the existing procedure of environmental protection agency (EPA) method 410.3. The detailed procedure is attached in Suplementary section.

3. Results and discussion

3.1. Analysis and characterization of the iron rusty waste

3.1.1. XRF data

The chemical composition of the rusty waste obtained from XRF analysis demonstrates that iron is the predominant element (51.50%w), which is similar to the data reported previously [34, 35]. Additionally, trace impurities of Cu (0.18 % w) and Zn (0.12 %w) are also detected, likely originating from environmental corrosion of the primary metal surface [33–35]. The other components (48.20 %w) undetectable by XRF method should be organic compounds, which are verified using an FTIR instrument.

3.1.2. FTIR data

FTIR analysis was conducted to confirm the presence of organic compounds in the rust waste, and the FTIR spectra is displayed in Fig. 1(a). In the spectra, absorption bands were observed at 470, 547, 1026, 1620, 2854, 2924, and 3433 cm^{-1}. The band observed at 547 cm^{-1} corresponds to $Fe-O$ stretching vibrations in hematite ($\alpha - Fe_2O_3$) [32, 34, 35], while the absorption at 476 cm^{-1} can be attributed to $Fe-O$ bonds in goethite (FeOOH) [34, 35]. In addition, several absorption bands (Supplementary section) were also detected to reflect the existence of organic compound that might be associated with the rust waste, the give evidence the assumption that addition of rusty waste has not free from organic compounds thus the iron composition of that cannot be a hundred percent.

3.2. Effect of the thermal treatment on the properties of iron oxide characters

3.2.1. Composition and crystallinity

The XRD pattern in Fig. 1(b) shows that the rust heated at 100 °C exhibits broad and less well-defined diffraction peaks with an irregular baseline and low intensity, whereas the rust heated at 450 °C displays sharper peaks with higher intensities. This indicates that at lower temperatures, the rusted material remains semi-crystalline, while higher crystallinity is achieved through calcination at elevated temperatures. In the diffraction pattern of the sample heated at 100 °C, distinct peaks appear at 2θ values of 30.01°, 35.45°, 57.14°, and 62.8°, which correspond to Fe_3O_4 (magnetite) with Miller indices (022), (113), (115), and (044), respectively, as listed in ICDD 96-900-5838 [18, 25, 32]. Additionally, peaks observed at 2θ values of 21.08°, 33.10°, and 41.93° are consistent with $\alpha - FeOOH$ (goethite), with Miller indices (101), (301), and (401), in agreement with ICDD 96-100-8767 [18, 32, 35, 39, 43]. These results clearly confirm the presence of a mixed-phase composition in the rusted iron heated at 100 °C.

Meanwhile, in the XRD pattern of the rusty waste calcined at 450 °C, peaks are observable at 20: 24.07°; 33.09°; 35.55°; 40.78°; 49.41°; 54.02°; 62.38°; 63.99°. The observed diffraction peaks can be unequivocally attributed to a single phase of $\alpha - Fe_2O_3$ (hematite), corresponding to the Miller indices (012), (104), (110), (113), (024), (116), (214), and (030), as documented in the ICDD database (96-9000140) and reported [18, 23, 29, 32, 34, 35, 39–41, 43, 44].

It is clearly shown that high-temperature calcination induces the phase transformation of goethite and magnetite into hematite, in accordance with the following reaction equations (6-7):

$$2FeOOH \rightarrow Fe_2O_3 + H_2O \tag{6}$$

$$2Fe_3O_4 + \frac{1}{2}O_2 \rightarrow 3Fe_2O_3 \tag{7}$$

3.2.2. Morphological evaluation

Scanning Electron Microscopy (SEM) characterization was conducted to examine the differences in surface morphology of iron rust waste dried at 100 °C and 450 °C. As shown in Fig. 2, the sample dried at 100 °C exhibits an agglomerated structure with indistinct shapes, which indicates a semicrystalline nature. In contrast, drying at the elevated temperature of 450 °C results in the formation of larger agglomerates with more clearly defined boundaries, suggesting the development of a crystalline phase [18]. These morphological observations are in good agreement with the XRD results, thereby confirming the phase evolution.

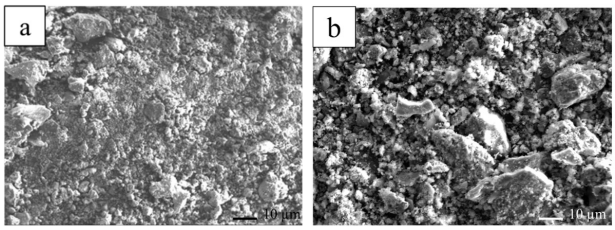

Fig. 2. The morphological features of the rusty waste heated at (a) 100 °C, and (b) 450 °C depict the structural alteration after thermal activation

3.2.3. UV-Vis DRS data

The spectra of UV-Vis DRS of both rust thermally treated at 100 and 450 °C, are displayed in Fig. 3, which is further

used to determine the band gap energy (Eg) of the iron oxides.

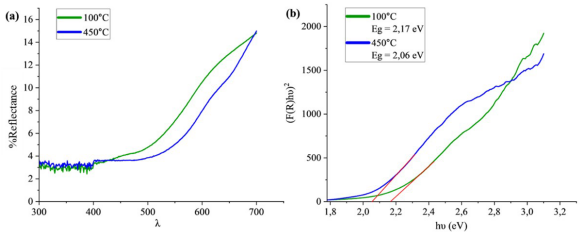

Fig. 3. (a) UV-Vis DRS spectra and (b) Tauc Plot of both rusty waste heated at 100 and 450 °C to evaluate and determine the band gap energy for the rusty wate as a heterogeneous catalyst in photo-Fenton process

The spectral data were analyzed using the Tauc plot method to determine the band gap energy (E_g), with the results presented in Fig. 3(b) Table 1S. As shown in the table, the mixture of goethite and magnetite obtained from heating iron rust at 100 °C exhibits a slightly larger band gap energy (Eg= 2.17 eV) compared to the sample calcined at the higher temperature of 450 °C (Eg = 2.06 eV), which corresponds to pure hematite. It is worth noting that $\alpha - FeOOH$ possesses a larger band gap (2.1-2.8 eV [18, 43], compared to that of Fe_3O_4 (0.1-0.2 eV) [18] and $\alpha - Fe_2O_3 (2.0 - 2.4\ eV)$ [18, 40, 43].

Upon heating at 100 °C, the material, which consists of a mixture of goethite and magnetite, exhibits a band gap higher than that of magnetite or hematite, indicating a significant contribution from goethite. At this lower temperature, the crystal structure remains incompletely developed, with OH bonds still present in goethite, thereby widening the effective band gap [18, 43]. In contrast, calcination at 450 °C produces single-phase hematite with enhanced crystallinity and stability, resulting in a narrower band gap of 2.06 eV. This value is consistent with that of pure hematite [18, 40, 43]. The lower band gap of Fe_2O_3 obtained at 450 °C compared to $FeOOH + Fe_3O_4$ at 100 °C is mainly due to phase transformation into hematite ($\alpha - Fe_2O_3$), improved crystallinity, removal of hydroxyl groups, and reduced quantum confinement effects. These structural and electronic changes make electron transitions easier, lowering the band gap energy [18, 43].

These findings suggest that rusty iron waste heated at both low and high temperatures exhibits semiconductor characteristics, making it a potential candidate for photocatalytic applications.

3.2.4. *Effect of thermal treatment on the surface parameters*

Fig. 4(a) shows that the isotherm curves of iron rust waste, both dried at 100 °C and calcined at 450 °C, correspond to type IV with an H3 hysteresis loop [18, 36, 45]. This indicates that the iron rust is a mesoporous material, characterized by pores with diameters ranging from 2 to 50 nm [36, 45], typically exhibiting slit-like or plate-shaped structures [45].

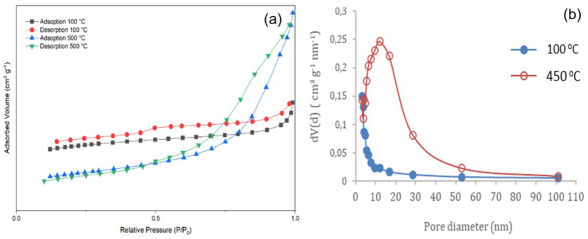

Fig. 4. (a) BET (Breuner Emmet Teller) Nitrogen adsorption isotherms, (b) pore size distributions of both iron rusty waste catalyst heated at 100 and calcined at 450 °C to evaluate the surface character of iron rusty waste catalyst

In addition to the adsorption-desorption isotherm curves, the pore size of the iron rust samples can also be analyzed from the Barrett-Joyner-Halenda (BJH) pore size distribution curves, as shown in Fig. 4(b). The pore size distribution of iron rust waste dried at 100 °C appears narrower, more homogeneous, and smaller, with an average size of approximately 4 nm. In contrast, the sample calcined at 450 °C exhibits a broader and more heterogeneous pore size distribution ranging from 3 to 30 nm, predominantly centered around 20 nm. Heating at 100 °C is sufficient only to remove the residual water trapped within the material, resulting in relatively small and uniform pores [31, 36, 39]. This narrow distribution is also attributed to the absence of sintering or grain growth processes at such a low temperature. Conversely, calcination at 450 °C promotes crystallization and sintering, during which particles begin to coalesce. This process partially closes smaller pores while simultaneously generating larger ones, thereby producing a wider pore size distribution with a dominant larger pore size [39].

From the BET analysis, the surface area, pore volume, and pore diameter were obtained and are presented in Table 1S. It can be observed that iron rust heated at 100 °C exhibits smaller surface area, pore volume, and pore diameter compared to the sample calcined at 450 °C. At 100 °C, the material consists of a semicrystalline mixture of FeOOH and Fe_3O_4, which tends to aggregate and form dense clus-

ters, thereby reducing the number of accessible pores as reflected in the lower pore volume. The incomplete dehydration and structural transformation at this low temperature result in a less porous morphology and consequently a smaller effective surface area [31, 36–38, 45, 46]. Meanwhile, heating at 450 °C leads to complete dehydration of FeOOH and transformation of Fe_3O_4 into crystalline Fe_2O_3. During calcination, the removal of hydroxyl groups and structural rearrangement generate more open pores and channels, yielding larger pore diameters and pore volumes. Despite the higher crystallinity, the particles are more effectively separated, reducing aggregation and enhancing porosity, which ultimately results in a greater specific surface area [31, 36–38, 45, 46].

3.3. Rusty catalyst test in the LAS photodegradation

3.3.1. Effect of thermal treatment of the catalyst on its activity

The catalytic activity of heated iron rusty waste in the photodegradation of LAS from laundry wastewater with an initial concentration of 119.18 mgL^{-1}, is displayed in Fig. 5. It can be observed that the catalyst heated at a higher temperature exhibits greater photodegradation efficiency compared to that treated at a lower temperature (Fig. 5(a)).

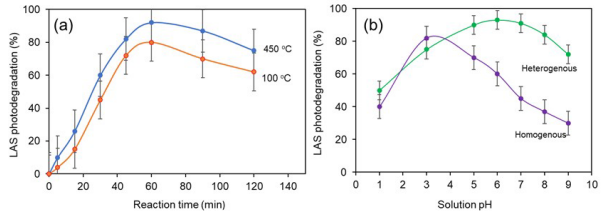

Fig. 5. (a) The effect of the thermal treatment on the catalyst activity under certain time exposure. It indicates the optimum reaction time of both calcination temperature variations is at 60 min. (b) The influence of solution pH on the LAS photodegradation was assessed using a heterogeneous and homogenous photocatalyst system during the photo-Fenton process

3.3.2. Mechanism of iron rusty waste as a heterogeneous photocatalyst in the photo Fenton process

The photodegradation obviously takes place through hydroxyl radicals attacking the organic molecules [1–18]. The formation of OH radicals in the heterogeneous photo-Fenton results from several reactions, as follows: i) between iron oxide, commonly presented as $\equiv Fe^{(III)} - OH$, with H_2O_2 (see reactions 8-10) [18, 19, 21, 29], ii. Between H_2O_2 with light (see reaction 3) [3, 7, 11, 12, 14–17, 25] and iii) between iron oxide that also acts as a photocatalyst with light (see reactions 11-13) [13, 18, 24, 30]. In reaction (9), $\cdot O_2H$ radicals are also generated, which exhibit weaker oxidizing activity compared to OH radicals [11].

$$\equiv Fe^{(III)} - OH + H_2O_2 \rightarrow \left[\equiv Fe^{(III)} - OH + H_2O_2\right]_s \rightarrow \equiv Fe^{(II)\cdot} \cdot O_2H + H^+ \quad (8)$$

$$\equiv Fe^{(II)\cdot O_2H \rightarrow Fe^{(II)} + \cdot O_2H} \quad (9)$$

$$\equiv Fe^{(II)} + H_2O_2 \rightarrow \equiv Fe^{(III)} - OH + \cdot OH \quad (10)$$

$$Fe_2O_3 + \text{ light } \rightarrow Fe_2O_3\left(h^+ + e^-\right) \quad (11)$$

$$h^+ + H_2O_2 \rightarrow H^+ + \cdot OH \quad (12)$$

$$e^- + O_2 \rightarrow \cdot O_2 \quad (13)$$

This data trend above is consistent with the corresponding values of band gap energy (E_g), surface area, pore volume, and pore diameter. With a band gap energy of approximately 2 eV, corresponding to a wavelength of about 600 nm in the visible light region, iron oxide as a photocatalyst can act as a semiconductor photocatalysts. This material is characterized by a valence band filled with electrons and an empty conduction band, separated by an energy gap known as the band gap energy (*Eg*). When this material is irradiated with UV or visible light, electrons are excited from the valence band into the conduction band, leaving behind holes in the valence band. These holes can react with hydroxide ions (OH^-) derived from water molecules to generate highly reactive hydroxyl radicals ($\cdot OH$). At the same time, the excited electrons in the conduction band can be captured by dissolved oxygen, forming superoxide radicals ($\cdot O_2$). This sequence of processes is illustrated schematically in Fig. 6 [2, 5, 6, 33–35].

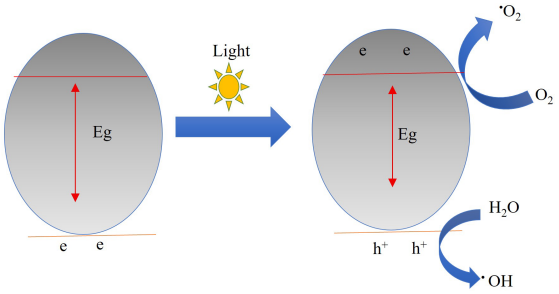

Fig. 6. Schematic mechanism on semiconductor photocatalyst structure and hydroxyl radical formation

A lower E_g enables the photocatalyst to absorb light more effectively, thereby generating a larger number of hydroxyl radicals responsible for degrading LAS molecules. Furthermore, photocatalysts with larger surface areas and higher pore volumes provide more active sites for pollutant

adsorption, which subsequently enhances their degradation efficiency [11, 13, 18, 31, 36]. The radical formation is also a result of the dissociation of H_2O_2 by light exposure, as seen in reaction (3).

To specifically distinguish the contribution of constituents in the photo-Fenton process, this research was also completed with additional experiments varying several parameters, as shown in Fig. 7.

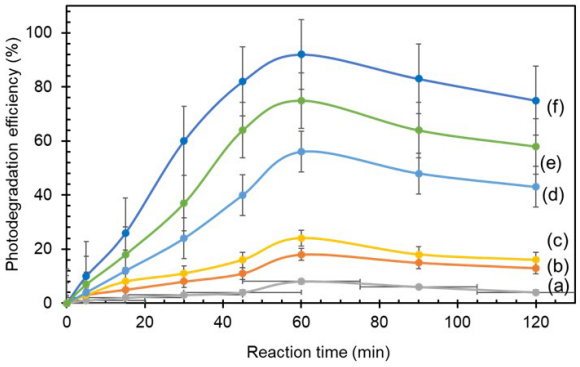

Fig. 7. Photodegradation efficiency of LAS in variations of parameters (a) LAS and iron rusty waste without UV illumination. (b) LAS with UV illumination only. (c) LAS and rusty waste with UV illumination. (d) LAS, rusty waste, H_2O_2 controlled in pH 5 (e) LAS and H_2O_2 with UV illumination. (f) LAS, H_2O_2, rusty waste, and UV illumination. All experiments are conducted using stirring for 60 min

According to these experiments, it can be seen clearly the contribution of each constituent. At first experiment (a), the presence of rusty waste that dominantly contained Fe_2O_3 could not produce the radicals as the fuel of the photo-degradation process. Thus, the percentage efficiency is very small. Some of the reduction of LAS concentration might be due to the possibility of adsorption on the Fe_2O_3 surface. Then, the presence of UV itself may actually break the organic molecules, including LAS, in the photolysis process (b). However, its efficiency is very low; without additional oxidizer, the OH from water photolysis inherited by the system remains limited. The combination with rusty waste and UV illumination (c) induces the photodegradation efficiency as UV could excite the electrons in Fe_2O_3, resulting in a hole to further oxidize water become OH radical. Even though that, the Fe_2O_3 has a high recombination degree, thus the excitation power for an electron remains low. Hence, the study of H_2O_2 through this system is evaluated in (d), which shows the substantial increase in LAS photodegradation efficiency. The decomposition of H_2O_2 itself can form the OH radicals aiding effectively by UV illumination (e). Furthermore, by employing Fe_2O_3 rusty waste, it became a heterogeneous catalyst that provides active sites for the Fe^{3+}/Fe^{2+} cycle (f). In this case, the UV illumination helps to boost the reduction process of Fe^{3+} to Fe^{2+}, thus ensuring the continuation of the Fenton cycle, and it can directly break the H_2O_2 oxidant into OH radical through the photolysis process. Hence, in the last system, it has two ways of radical formation. First, from the direct photolysis of H_2O_2 by UV illumination. Second, the Fenton reaction is strengthened by the photoreduction of Fe^{3+}. It anticipated the eminent mechanism in comparison with the conventional photo-Fenton process, as it offers more OH radicals and fast Fe^{2+} regeneration, thus preventing the bottleneck in Fenton cycles, ensuring the effectiveness of the Fenton process to generate the radicals.

3.3.3. *Effect of Irradiation Time*

As also illustrated in Fig. 6, the degradation of LAS progressively increases with the extension of reaction time, attaining its maximum efficiency at 60 minutes. This behavior can be attributed to the progressive generation of hydroxyl radicals and their increasingly effective interaction with LAS molecules. However, extending the reaction time beyond this optimum slightly decreases the degradation efficiency, which may be due to catalyst surface saturation that limits further OH radical formation. Additionally, prolonged exposure may promote recombination of intermediate radicals, thereby reducing the overall number of active OH radicals available for LAS degradation [3, 7, 8, 11, 12, 14–17, 20–22, 24, 27–31].

To gain detail investigation, the data on the influence of the irradiation time was also processed to study the kinetic models. Based on the data presented in the Supplementary materials (Fig 1S), it is well-accepted that iron rusty waste obeys the pseudo-first order, as it yields the greatest R^2 value. Both the photo-Fenton process that uses iron rusty waste catalyst heated at 100 °C or calcinated at 450 °C follow the pseudo-first order. This behavior was relevant to the common photo-Fenton process in previous results [47–49]. It tends to imply that during the photo-Fenton process, using rusty waste photo-catalyst depends only on the pollutant concentrations, since the OH radicals are excessive. According to the slope in Fig 1S for pseudo-first order kinetic fitting, the k (kinetic constant variable) is 0.0527 min^{-1} and 0.0243 min^{-1} for high temperature calcination and low temperature calcination of iron rusty waste, respectively. Further discussion regarding effect of irradiation time is found in Supplementary materials.

3.3.4. *Effect of pH*

Fig. 5(b) illustrates the photodegradation of LAS through both homogeneous and heterogeneous photo-Fenton processes at different pH values. The figure shows that in the homogeneous photo-Fenton process, LAS degradation is less effective under highly acidic conditions. The efficiency reaches its maximum at pH 3 and decreases progressively with increasing pH. Some papers reported similar findings [8, 11, 12, 14–17].

At pH values below 3, the excessively acidic environment promotes the formation of stable complexes of iron ions $\left(Fe^{2+}/Fe^{3+}\right)$, such as $[Fe\,(H_2O)_6]^{2+}$ and $[Fe\,(H_2O)_6]^{3+}$ which limits their participation in the catalytic cycle [8, 11, 12, 14–17]. Moreover, hydrogen peroxide (H_2O_2) becomes more stable under these conditions, as the high proton concentration (H^+) suppresses its decomposition into water and oxygen [8, 11, 12, 14–17]. Consequently, fewer hydroxyl radicals (·OH) are generated, reducing the overall degradation efficiency. An increase in pH up to 3 maintains Fe^{2+} in a soluble and active state, allowing efficient cycling between Fe^{2+} and Fe^{3+} under UV/visible irradiation [8, 11, 12, 14–17]. Consequently, hydroxyl radicals are generated at the highest rate, leading to maximum LAS degradation. At this pH, both iron solubility and H_2O_2 stability are optimally balanced [8, 11, 12, 14–17], ensuring effective radical production. However, at pH values above 3, Fe^{3+} ions tend to precipitate as ferric hydroxide $[Fe(OH)_3]$, thereby reducing the availability of soluble Fe^{2+}/Fe^{3+} species for the catalytic cycle [11, 15–17]. This precipitation diminishes the concentration of active species and lowers hydroxyl radical generation, ultimately rendering the photo-Fenton process less effective in LAS degradation. Further discussion regarding effect of pH is found in Supplementary materials.

3.3.5. *Effect of H_2O_2 Concentration*

As shown in Fig. 8(a), increasing the H_2O_2 concentration up to 250 mmolL^{-1} enhances LAS degradation, primarily due to the greater formation of hydroxyl radicals (·OH). However, beyond this concentration, the degradation efficiency decreases because excess H_2O_2 acts as a scavenger of ·OH radicals, leading to the formation of less reactive hydroperoxyl radicals ($HO_2^{\cdot}$) [8, 11, 12, 14–17], as illustrated in reaction (14). Previous reports obtained a similar data trend [8, 11, 12, 14–17]. The determination of H_2O_2 is really important to ensure the effectiveness of the photo-Fenton process using a heterogeneous catalyst. Since the photo-Fenton reaction is applied for treating wastewater with massive loads of contaminants, it needs the external addition of large amounts of H_2O_2. The optimization of H_2O_2 dosage can reduce the operational cost of photo-Fenton, which will increase the efficiency of photo-Fenton process [50]. Thus, in this research, the relatively high amount of H_2O_2 is based on several experiments to gain the optimum condition and efficient photo-Fenton process.

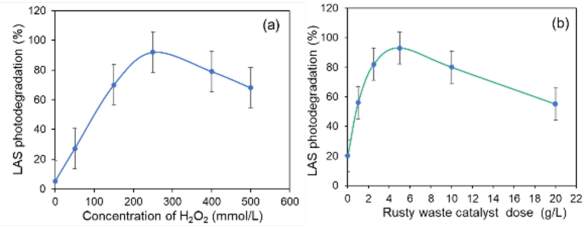

Fig. 8. Influence of (a) the H_2O_2 concentration and (b) catalyst dose, on the 10 mL LAS photodegradation using rusty waste at 6 g L^{-1}

$$H_2O_2 + OH \rightarrow H_2O + HO_2^{\cdot} \tag{14}$$

The detailed explanation is deliverd in Supplementary section.

3.3.6. *Effect of Catalyst Dosage*

Figure 8(b) illustrates the influence of catalyst dosage, showing that increasing the catalyst amount enhances LAS photodegradation, with maximum efficiency achieved at 6 g L^{-1} of rusty waste as Fe_2O_3, corresponding to an Fe dosage of 0.75 mmolL^{-1} or 2830 mgL^{-1}. This trend data is consistent with findings reported in previous studies [19–22, 24–29, 31]. The increase in catalyst mass provides a greater number of active sites and promotes the generation of additional hydroxyl radicals (·OH), thereby facilitating more effective LAS degradation. However, when the dosage exceeds the optimum level, the opposite trend is observed. This decline in efficiency is attributed to increased turbidity, which reduces UV light penetration and consequently limits hydroxyl radical (·OH) generation. Further discussion regarding catalyst dosage and COD analysis are found in Supplementary materials.

4. Conclusion

The research results conclude that the heterogeneous photo-Fenton process using a rust-based catalyst is more effective for LAS photodegradation at near-neutral pH (5-7) compared to the homogeneous photo-Fenton process. Rusty waste heated at 100 °C was found to consist of a semicrystalline mixture of FeOOH and Fe_3O_4, which transforms into single-phase crystalline Fe_2O_3 upon calcination at 450 °C. The material calcined at 450 °C exhibits a lower band

gap energy (*Eg*), along with a larger surface area, pore volume, and pore diameter than the sample treated at 100 °C. In line with these enhanced physicochemical properties, the 450 °C calcined rusty waste demonstrates superior photocatalytic performance in degrading LAS compared to the 100 °C treated material. The optimum conditions for heterogeneous photo-Fenton catalysis using Fe_2O_3 derived from rusty waste calcined at 450 °C were achieved with a catalyst dosage of 6 g L^{-1}, H_2O_2 concentration of 250 mmolL^{-1}, reaction time of 60 minutes, and pH 6. Under these conditions, a photodegradation efficiency of 95% was obtained for 119.08 mgL^{-1} LAS in 50 mL of laundry wastewater.

5. Acknowledgement

The authors would like to express their sincere gratitude to Universitas Gadjah Mada for supporting this research through the Final Project Recognition (RTA) funding scheme under contract number 5286/tNl.P1/PT.01.03/2024, dated May 6, 2024.

References

[1] V. V. Patil, P. R. Gogate, A. P. Bhat, and P. K. Ghosh, (2020) *"Treatment of laundry wastewater containing residual surfactants using combined approaches based on ozone, catalyst and cavitation"* **Separation and Purification Technology** ***239***: 116594. DOI: https://doi.org/10.1016/j.seppur.2020.116594.

[2] E. T. Wahyuni, I. Istiningsih, and A. Suratman, (2020) *"Use of visible light for photo degradation of linear alkylbenzene sulfonate in laundry wastewater over Ag-doped TiO2."* ***13***: 124–130. DOI: 10.3923/jest.2020.124.130.

[3] E. T. Wahyuni, A. Sabrina, and N. H. Aprilita, (2022) *"Enhancement of Fenton Performance at Near-Neutral pH by Using Ethylene Diamine Tetra Acetic Acid for Anionic Surfactant Removal from a Laundry Wastewater"* **Key Engineering Materials** ***920***: 57–62. DOI: 10.4028/p-6652l7.

[4] E. Sugiharto, (2014) *"Distribution of Detergent Waste in the Environment and the Removal by Using Photocatalytic Degradation and Coagulation Methods"* **American Chemical Science Journal** ***4***: 715–725.

[5] N. A. Affandi, C. G. Joseph, M. I. Nabeel, M. Hafiz, A. Majid, and K. Ghazali, (2025) *"Photolytic and Photocatalytic Degradation of Detergent and Surfactant Solutions by Various Light Sources"* **Malaysian Journal of Chemistry** ***27***: 41–63. DOI: https://doi.org/10.55373/mjchem.v27i6.41.

[6] M. E.-D. R. Hassan, M. E. S. Barakat, and E. H. E. Yosef, (2024) *"Synthesis and evaluation of core–shell nanocomposites for the photodegradation of liner alkylbenzene sulfonate water contaminations"* **International Journal of Environmental Science and Technology** ***21***: 3185–3200. DOI: 10.1007/s13762-023-05181-4.

[7] M. B. Miranzadeh, R. Zarjam, R. Dehghani, M. Haghighi, H. Z. Badi, M. A. Marzaleh, and A. M. Tehrani, (2016) *"Comparison of fenton and photo-fenton processes for removal of linear alkyle benzene sulfonate (LAS) from aqueous solutions"* **Pol. J. Environ. Stud** ***25***(4): 1639–1648. DOI: /10.15244/pjoes/61824.

[8] E. T. Wahyuni, R. Roto, M. Sabrina, V. Anggraini, N. F. Leswana, and A. C. Vionita, (2016) *"Photodegradation of Detergent Anionic Surfactant in Wastewater Using UV/TiO_2/H_2O_2 and UV/Fe^{2+}/H_2O_2 Processes"* **American Journal of Applied Chemistry** ***4***(5): 174–180. DOI: 10.11648/j.ajac.20160405.13. eprint: https://article.sciencepublishinggroup.com/pdf/10.11648.j.ajac.20160405.13.

[9] M. Bradai, J. Han, A. E. Omri, N. Funamizu, S. Sayadi, and H. Isoda, (2014) *"Cytotoxic effect of linear alkylbenzene sulfonate on human intestinal Caco-2 cells: associated biomarkers for risk assessment"* **Environmental Science and Pollution Research** ***21***: 10840–10851. DOI: 10.1007/s11356-014-3074-6.

[10] K. Wysokowska, Z. Cupiał, M. Staszak, A. Zgoła-Grześkowiak, J. Koziolek, Ł. Ławniczak, M. Wysokowski, and B. Wyrwas, (2024) *"Photocatalytic degradation of non-ionic, anionic, and cationic surfactants: from batch experiments through equilibrium/kinetic study to ecotoxicology analysis"* **Chemical Papers** ***78***: 761–777. DOI: 10.1007/s11696-023-03117-3.

[11] M.-h. Zhang, H. Dong, L. Zhao, D.-x. Wang, and D. Meng, (2019) *"A review on Fenton process for organic wastewater treatment based on optimization perspective"* **Science of The Total Environment** ***670***: 110–121. DOI: https://doi.org/10.1016/j.scitotenv.2019.03.180.

[12] G. Papadopoulou, E. Evgenidou, and D. Lambropoulou, (2025) *"Homogeneous and Heterogeneous Photo-Fenton-Based Photocatalytic Techniques for the Degradation of Nile Blue Dye"* **Applied Sciences** ***15***(14): DOI: 10.3390/app15147917.

[13] H. Befenzi, A. Ezzariai, T. Mechichi, L. Kouisni, M. Hafidi, E. Record, and L. EL Fels, (2025) *"Degradation of antibiotics by homogeneous and heterogeneous Fenton processes: A review"* **Journal of Hazardous Materials**

Advances *17*: 100522. DOI: https://doi.org/10.1016/j.hazadv.2024.100522.

[14] A. Vishwanath and Vaidya. "Comparison Of Different Advanced Oxidation Processes For 2-Nitrophenol (2-NP) Degradation In Aqueous Solution". In: 2023.

[15] E. T. Wahyuni, A. Nurhikmatillah, H. Kurniasari, and D. Siswanta, (2021) *"Detoxification of as(III) in aqueous media by using photo-Fenton method."* ***23***: 550–555. DOI: 10.30955/gnj.003265.

[16] E. T. Wahyuni, D. Siswanta, E. S. Kunarti, D. Supraba, and S. Budiraharjo, (2019) *"Removal of Pb(II) ions in the aqueous solution by photo-Fenton method"* **Global Nest Journal *21***: 180–186. DOI: 10.30955/gnj.002936.

[17] A. Mirzaei, Z. Chen, F. Haghighat, and L. Yerushalmi, (2017) *"Removal of pharmaceuticals from water by homo/heterogonous Fenton-type processes – A review"* **Chemosphere *174***: 665–688. DOI: 10.1016/j.chemosphere.2017.02.019.

[18] A. Choquehuanca, J. G. Ruiz-Montoya, and A. L. R.-T. Gómez, (2021) *"Discoloration of methylene blue at neutral pH by heterogeneous photo-Fenton-like reactions using crystalline and amorphous iron oxides"* **Open Chemistry *19***(1): 1009–1020. DOI: 10.1515/chem-2021-0077.

[19] J. A. S. Ribeiro, J. F. Alves, B. C. B. Salgado, A. C. Oliveira, R. S. Araújo, and E. Rodríguez-Castellón, (2024) *"Heterogeneous Photo-Fenton Degradation of Azo Dyes over a Magnetite-Based Catalyst: Kinetic and Thermodynamic Studies"* **Catalysts *14***(9): DOI: 10.3390/catal14090591.

[20] L. Martinez, H. Gomes, G. Drazic, J. Faria, and A. Silva, (2014) *"Hydrothermal synthesis of iron oxide photo-Fenton catalysts: The effect of parameters on morphology, particle size and catalytic efficiency"* **Global Nest Journal *16***: 474–484.

[21] A. Shokri and M. S. Fard, (2023) *"Using α-Fe_2O_3/SiO_2 as a heterogeneous Fenton catalyst for the removal of chlorophenol in aqueous environment: Thermodynamic and kinetic studies"* **International Journal of Environmental Science and Technology *20***: 383–396. DOI: 10.1007/s13762-022-04498-w.

[22] H. Rasouli, M. Khodabakhshi, and M. Ghorbanpour, (2022) *"Decolorization of methyl orange dye by photo-Fenton process using silica gel/iron oxide catalyst"* **Desalination and Water Treatment *274***: 289–296. DOI: 10.5004/dwt.2022.28919.

[23] A. Magomedova, A. Isaev, F. Orudzhev, D. Sobola, R. Murtazali, A. Rabadanova, N. S. Shabanov, M. Zhu, R. Emirov, S. Gadzhimagomedov, N. Alikhanov, and K. Kasinathan, (2023) *"Magnetically Separable Mixed-Phase α/γ-Fe_2O_3 Catalyst for Photo-Fenton-like Oxidation of Rhodamine B"* **Catalysts *13***(5): DOI: 10.3390/catal13050872.

[24] M. Ahmad, A. R. A. Aziz, S. A. Mazari, A. G. Baloch, and S. Nizamuddin, (2020) *"Photocatalytic degradation of methyl orange from wastewater using a newly developed Fe-Cu-Zn-ZSM-5 catalyst"* **Environmental Science and Pollution Research *27***: 26239–26248. DOI: 10.1007/s11356-020-08940-9.

[25] J. Xu, Q. Ma, W. Feng, X. Zhang, Q. Lin, C. You, and X. Wang, (2022) *"Removal of methyl orange from water by Fenton oxidation of magnetic coconut-clothed biochar"* **RSC advances *12***(38): 24439–24446. DOI: 10.1039/D2RA03545F.

[26] I. Ouiriemmi, A. Karrab, N. Oturan, M. Pazos, E. Rozales, A. Gadri, M. Á. Sanromán, S. Ammar, and M. A. Oturan, (2017) *"Heterogeneous electro-Fenton using natural pyrite as solid catalyst for oxidative degradation of vanillic acid"* **Journal of Electroanalytical Chemistry *797***: 69–77. DOI: 10.1016/j.jelechem.2017.05.028.

[27] N. Barhoumi, H. Olvera-Vargas, N. Oturan, D. Huguenot, A. Gadri, S. Ammar, E. Brillas, and M. A. Oturan, (2017) *"Kinetics of oxidative degradation/mineralization pathways of the antibiotic tetracycline by the novel heterogeneous electro-Fenton process with solid catalyst chalcopyrite"* **Applied Catalysis B: Environmental *209***: 637–647. DOI: 10.1016/j.apcatb.2017.03.034.

[28] M. Ioffe, S. Kundu, N. Perez-Lapid, and A. Radian, (2022) *"Heterogeneous Fenton catalyst based on clay decorated with nano-sized amorphous iron oxides prevents oxidant scavenging through surface complexation"* **Chemical Engineering Journal *433***: 134609. DOI: 10.1016/j.cej.2022.134609.

[29] A. Özcan, A. Atılır Özcan, Y. Demirci, and E. Şener, (2017) *"Preparation of Fe2O3 modified kaolin and application in heterogeneous electro-catalytic oxidation of enoxacin"* **Applied Catalysis B: Environmental *200***: 361–371. DOI: 10.1016/j.apcatb.2016.07.018.

[30] S. Filice, C. Bongiorno, S. Libertino, L. Gradon, D. Iannazzo, and S. Scalese, (2022) *"Photo-Fenton Degradation of Methyl Orange with Dunino Halloysite as a Source of Iron"* **Catalysts *12***(3): DOI: 10.3390/catal12030257.

[31] X. Liu, H.-L. Liu, K.-P. Cui, Z.-L. Dai, B. Wang, and X. Chen, (2022) *"Heterogeneous Photo-Fenton Removal of Methyl Orange Using the Sludge Generated in Dyeing Wastewater as Catalysts"* **Water *14***(4): DOI: 10.3390/w14040629.

[32] H. Ghazzaf, B. Nechchadi, A. Jouali, A. Salhi, M. El Krati, and S. Tahiri, (2022) *"Synthesis of heterogeneous photo-Fenton catalyst from iron rust and its application to degradation of Acid Red 97 in aqueous medium"* **Journal of Environmental Chemical Engineering *10***(3): 107570. DOI: 10.1016/j.jece.2022.107570.

[33] E. T. Wahyuni, N. D. Lestari, I. R. Cinjana, S. Annur, T. A. Natsir, and M. Mudasir, (2023) *"Doping TiO2 with Fe from iron rusty waste for enhancing its activity under visible light in the Congo red dye photodegradation"* **Journal of Engineering and Applied Science *70***: 9. DOI: 10.1186/s44147-023-00178-9.

[34] E. T. Wahyuni, S. Annur, N. D. Lestari, and M. Mudasir, (2024) *"Conversion of iron rusty waste into Fe dopant of TiO2 to increase its photocatalytic activity under visible light for photodegradation of rhodamine-B"* **Results in Engineering *22***: 102296. DOI: 10.1016/j.rineng.2024.102296.

[35] K. KHOIRUNISA, N. D. LESTARI, E. T. WAHYUNI, and T. A. NATSIR, (2025) *"Enhanced photocatalytic reduction of Cr(VI) under visible light a magnetically separable TiO_{2}-$Fe/Fe_{3}O_{4}$ photocatalyst prepared from iron rusty waste"* **Journal of Metals, Materials and Minerals *35***: e2162. DOI: 10.55713/jmmm.v35i1.2162.

[36] T. Jiang, A. S. Poyraz, A. Iyer, Y. Zhang, Z. Luo, W. Zhong, R. Miao, A. M. El-Sawy, C. J. Guild, Y. Sun, D. A. Kriz, and S. L. Suib, (2015) *"Synthesis of Mesoporous Iron Oxides by an Inverse Micelle Method and Their Application in the Degradation of Orange II under Visible Light at Neutral pH"* **The Journal of Physical Chemistry C *119***(19): 10454–10468. DOI: 10.1021/acs.jpcc.5b02057.

[37] H. Lee, H. S. Jang, N. Y. Kim, and J. B. Joo, (2021) *"Cu-doped TiO2 hollow nanostructures for the enhanced photocatalysis under visible light conditions"* **Journal of Industrial and Engineering Chemistry *99***: 352–363. DOI: 10.1016/j.jiec.2021.04.045.

[38] S. Kaufhold, R. Dohrmann, I. Wallis, and C. Weber, (2023) *"Chemical and mineralogical reactions of bentonites in geotechnical barriers at elevated temperatures: review of experimental evidence and modelling progress"* **Clay Minerals *58***(3): 280–300. DOI: 10.1180/clm.2023.26.

[39] L. Frolova. "Studying of iron oxyhydroxide dehydration". In: *International Conference on Nanotechnology and Nanomaterials*. Springer. 2020, 165–169.

[40] J. Khanam, M. R. Hasan, B. Biswas, M. F. Ahmed, S. Mostofa, U. S. Akhtar, M. K. Hossain, M. S. Quddus, S. Ahmed, N. Sharmin, and S. M. Al-Reza, (2024) *"Effect of low temperature calcination on micro structure of hematite nanoparticles synthesized from waste iron source"* **Heliyon *10***: DOI: 10.1016/j.heliyon.2024.e41030.

[41] M. Zhong, Y. He, E. A. Milligan, P. C. Pistorius, and B. A. Webler, (2020) *"In Situ Observation of Reaction Fronts During the Initial Stages of Iron Surface Oxidation at 1150 °C"* **Oxidation of Metals *93***: 449–463. DOI: 10.1007/s11085-020-09965-8.

[42] S. Rawat, K. R. Singh, and J. Singh, (2025) *"Synthesis of iron nanoparticles using iron recovered from rust: An application for the catalytic degradation of phenols"* **Environmental Science and Pollution Research**: DOI: 10.1007/s11356-025-36114-y.

[43] L. Boumaza, S. Boudjadar, O. Abdelaziz, A. Mougari, M. Zabat, and Y. Aouabdia, (2025) *"Eco-friendly synthesis of iron oxide nanoparticles (IO-NPs): grain size and strain estimation models, band gap calculations, and antibacterial properties"* **Physics and Chemistry of Minerals *52***: 29. DOI: 10.1007/s00269-025-01332-w.

[44] A. H. Kadhim and N. B. Hasan, (2019) *"Structural and morphological properties of Fe2O3 and TiO2: Fe2O3 thin films prepared by spray pyrolysis technique"* **Journal of Kufa-Physics *11***(1): 27–34. DOI: 10.31257/2018/JKP/2019/110105.

[45] K. Jiang, J. Zhang, R. Luo, Y. Wan, Z. Liu, and J. Chen, (2021) *"A facile synthesis of Zn-doped TiO2nanoparticles with highly exposed (001) facets for enhanced photocatalytic performance"* **RSC Advances *11***: 7627–7632. DOI: 10.1039/d0ra09318a.

[46] N. Thomas, D. D. Dionysiou, and S. C. Pillai, (2021) *"Heterogeneous Fenton catalysts: A review of recent advances"* **Journal of Hazardous Materials *404***: 124082. DOI: 10.1016/j.jhazmat.2020.124082.

[47] K. O'Dowd and S. C. Pillai, (2020) *"Photo-Fenton disinfection at near neutral pH: Process, parameter optimization and recent advances"* **Journal of Environmental Chemical Engineering *8***: DOI: 10.1016/j.jece.2020.104063.

[48] E. Ortega-Gómez, P. Fernández-Ibáñez, M. M. B. Martín, M. I. Polo-López, B. E. García, and J. A. S. Pérez, (2012) *"Water disinfection using photo-Fenton: Effect of temperature on Enterococcus faecalis survival"* **Water Research *46***: 6154–6162. DOI: 10.1016/j.watres.2012.09.007.

[49] N. Mukwevho, P. J. Mafa, K. K. Kefeni, A. K. Mishra, S. B. Mishra, and A. T. Kuvarega, (2024) *"Photo-Fenton like reaction for the degradation of methyl orange using magnetically retrievable NiFe2O4/CoMoS4 heterojunction photocatalyst"* **Journal of Water Process Engineering *65***: DOI: 10.1016/j.jwpe.2024.105882.

[50] N. Thomas, D. D. Dionysiou, and S. C. Pillai, (2021) *"Heterogeneous Fenton catalysts: A review of recent advances"* **Journal of Hazardous Materials *404***: DOI: 10.1016/j.jhazmat.2020.124082.